From transistors to phototransistors by tailoring the polymer stacking

Shuaiwei Cui,[a] Dongxu Liang,[a] Maning Liu,[b] Paola Vivo,[b] Meng Zheng,[a] Tao Zhuang,[a] Qikun Sun,[a] Wenjun Yang,[a] Haichang Zhang[a]*

[a]Key Laboratory of Rubber-Plastics of Ministry of Education/Shandong Province (QUST), School of Polymer Science & Engineering, Qingdao University of Science & Technology, 53-Zhengzhou Road, Qingdao, 266042, PR China

[b]Hybrid Solar Cells, Faculty of Engineering and Natural Sciences, Tampere University, P.O. Box 541, Tampere FI-33014, Finland

Corresponding author: Haichang Zhang: haichangzhang@hotmail.com

ABSTRACT

It is universally acknowledged that highly photosensitive transistors are strongly dependent on the high carrier mobility of polymer-based semiconductors. However, the polymer π-π stacking and aggregation, required to increase the charge mobility, conversely inhibit the dissociation of photogenerated charge carriers, in turn accelerating the geminate recombination of electron-hole pairs. To explore the effects of charge mobility and polymer stacking on the photoresponsivity of the phototransistors, here, we synthesize two alternating copolymers, namely P-PPAB-IDT

and P-PPAB-BDT, by Palladium-catalyzed Stille coupling of PPAB with IDT or BDT monomers. The polymer P-PPAB-IDT demonstrates a nearly 20 times enhancement in the hole mobility compared to P-PPAB-BDT. Yet, P-PPAB-IDT surprisingly shows no response to white light illumination, whereas P-PPAB-BDT exhibits a significant photoresponse to the same light source with a high light-current/dark-current (I_{light}/I_{dark}) ratio of 21.6 in the p-type area and a low current ratio of just 5.2 in the n-type area. We believe that this work will provide an effective strategy to develop highly photosensitive polymer semiconductors by reducing the polymer stacking and aggregation rather than improving the charge carrier mobility.

1. Introduction

Phototransistors (PTs), as an emerging type of optical transducers based on field-effect transistors (FETs), have recently demonstrated a great potential for multiple optoelectronic applications, such as optoisolators, retro-sensors, and optoelectronic switches.[1-4] Phototransistors integrate the light-detection capability of photodiodes with the signal-amplification function of transistors, thus exhibiting higher photosensitivity and lower noise levels than conventional photodiodes and photoconductors.[5-10] Although inorganic phototransistors (e.g., single crystalline silicon and InAlAs-InGaAs) have attracted considerable attention from both the industry and the global market, the high-temperature processing under vacuum, the poor compatibility with flexible

substrates, and the limited sensing areas significantly restrict their further developments and practical applications.[11,12] Therefore, realizing low-cost, high-sensitivity, and highly flexible phototransistors in a large-scale area has quickly become an important research focus.

Conjugated polymers (CPs) are well-known and promising candidates for solution-processable and cost-effective semiconductor materials due to several attractive merits, including intrinsic flexibility, incorporation of functionality via molecular design, and ease of achieving large-scale and low-cost device fabrication through facile methods, such as spin coating, drop-casting, and inkjet printing.[13-17] In recent years, although the rational tuning of the electronic energy levels and band gaps is widely investigated, the charge carrier mobility of the reported CPs is still much lower than that of amorphous silicon (≈ 1 cm^2 V^{-1} s^{-1}). Extensive studies have demonstrated that the wide absorption band of CPs determines the efficient photoinduced charge carrier generation under illumination, while the high charge carrier mobility ensures the swift charge transport and collection at the electrodes.[18-20] However, the strong π-π packing and high exciton binding energy (0.3-1 eV) desirable when aiming to high mobility of the CPs are generally detrimental for their use as the photoactive layer in the phototransistors.[21-22] Thus, how to balance the π-π packing and charge carrier mobility of the CPs is of crucial significance for fabricating high-performance phototransistors.

Recent reports have demonstrated that diketopyrrolopyrrole (DPP)-based CPs are considered as highly prospective photoactive materials for solution-processed organic optoelectronic devices like organic solar cells (OSCs) and organic FETs (OFETs).[23-27] By selectively amalgamating the electron-deficient DPP units with proper electron-rich units, the D-A copolymers could show good planarity, controllable conjugated system, adjustable energy level, high charge carrier mobility, high thermal stability as well as fabulous solution processability. Nevertheless, DPP or its derivative-based materials are widely used in OFETs but rarely in phototransistors. One DPP unit contains two amide moieties that endow it with strong electron-withdrawing ability.[28,29] The amide units could further be functionalized with the pyrrolopyrrole aza-BODIPY (PPAB) (see Scheme 1). Compared to the DPP, the PPAB units may exhibit broad optical absorption in the visible-to-near infrared (NIR) region due to the better π-conjugation extension, and the unique heteroaromatic amines, i.e., double B←N bridge bond and fluorine atoms. In addition, the existence of fluorine atoms can efficiently deepen the LUMO energy levels and improve the molecular packing of PPAB-containing conjugated polymers, which is responsible for the high charge carrier mobility. To the best of our knowledge, there are only two articles that previously involved the synthesis of PPAB-based materials. In 2014, Wiktorowski *et al.* reported a synthetic route regarding the substitution of benzothiazole and quinoline unites by small PPAB molecules, which

shows strong optical absorption in the NIR region ranging from 800 to 1200 nm.[30] Subsequently, Furuta's group designed the PPAB dimers and applied them as the light absorber in OSCs, which achieved a power conversion efficiency (PCE) of about 0.74 %.[31] However, to date, the photoelectrical applications of the PPAB-containing CPs have only attracted very limited attention. In this work, we have designed and successfully synthesized two novel conjugated polymers, namely P-PPAB-IDT and P-PPAB-BDT, based on PPAB as the electron-withdrawing unit and distannylated indacenodithiophene (IDT) or benzo[1,2-b:4,5-b']dithiophene-2,6-diyl) (BDT) as the electron-rich unit. The effects of π-π molecular stacking and charge carrier mobility of the conjugated polymers on the optical, electrochemical, and thermal properties as well as on the photoelectronic performance, have been systematically investigated. Surprisingly, compared with the charge carrier mobility of the conjugated polymers, the π-π stacking plays a dominant role in the photoswitching characteristics of the as-prepared transistors. We found that the strong charge transport unbalance indeed triggers a photoconductive gain mechanism, resulting in efficient photocurrent generation and dissociation only in the case of BDT-based phototransistors. This work provides insight into the synthesis of highly photosensitive conjugated polymers by rationally manipulating the polymer π-π stacking, and pioneers the application of PPAB-based conjugated polymers in phototransistors.

2. Results and discussion

2.1 Polymer Synthesis

The two novel D-A conjugated copolymers, P-PPAB-IDT and P-PPAB-BDT, were synthesized according to Scheme 1 by utilizing the Stille coupling polymerization, and purified with standard Soxhlet extraction procedure. The PPAB monomer was synthesized via a Schiff-base reaction of diketopyrrolopyrrle and heteroaromatic amines with a 28 % yield.[31] The PPAB monomer was characterized by $^{1}H/^{13}C$ NMR, elemental analysis, and mass spectroscopy while the two polymers were characterized by ^{1}H NMR and gel permeation chromatography (GPC). The NMR spectra of the compounds exhibit all the expected resonance peaks. The proton signals on the alkyl chain are between 0.78 and 1.5 ppm, while the signals between 7.0 and 8.4 ppm are assigned to the protons from the aromatic ring units. According to the GPC with *N*, *N*-dimethylformamide as the eluent at 60 ºC, the weight-average molecular weight (M_w) of P-PPAB-IDT and P-PPAB-BDT are 16 and 19.3 kDa, and the polydispersity indices (PDI) of two cases were 2.5 and 2.8, respectively. Both polymers present a good solubility in most common organic solvents such as toluene and chloroform, which is beneficial for the solution-processed fabrication of the corresponding electronic devices. For both polymers, the PPAB groups function as the electron-withdrawing units, while the IDT or BDT units act as the electron-donating moieties, thus resulting in a donor-

acceptor (D-A) system with intramolecular charge transfer (ICT) effect. This effect is highly beneficial for promoting both intramolecular delocalization and intermolecular dipole-dipole interactions.[32-34] The thermal stability of the two polymers was investigated by thermogravimetric analysis (TGA) and differential scanning chromatography (DSC). As seen in Figure S1a in the Supporting Information (SI), both polymers show a thermal transition at around 69 ºC, possibly attributed to the vibration of the alkyl chain attached to the polymer backbone. However, between 25 and 260 ºC, there is no obvious melting peak as well as glass transition temperature (T_g). This means that, compared to the crystalline structure, the amorphous film indeed dominates the phase. No glass transition is detected, potentially due to the rigid polymer backbone. The TGA spectra reveal that there is no weight loss before 300 °C for both polymers, and the 5% weight loss occurs at 334 °C and 316 °C for P-PPAB-IDT and P-PPAB-BDT, respectively, indicative of high thermal stability achieved in each case (Figure S1b).

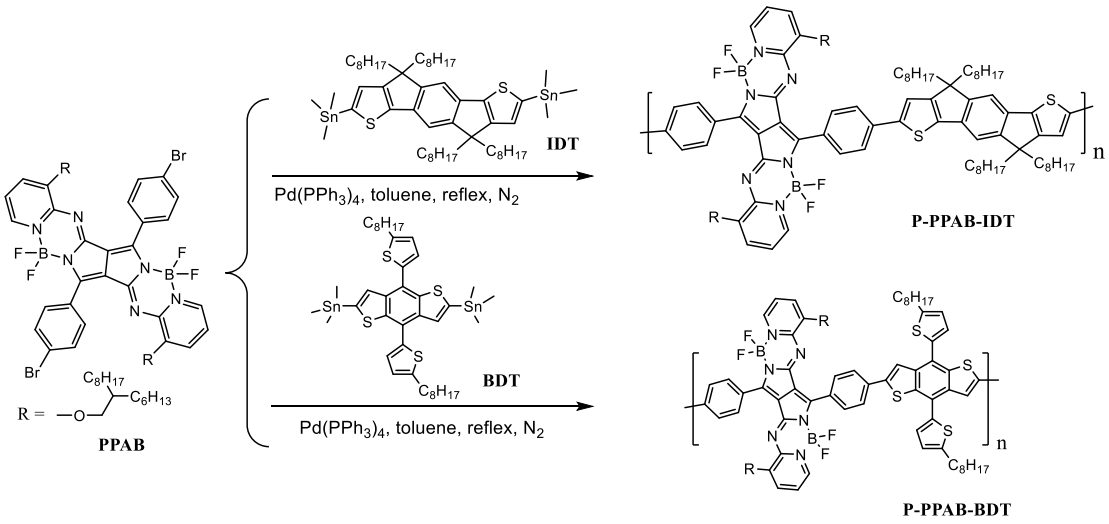

Scheme 1. Synthetic routes of the two P-PPAB-IDT and P-PPAB-BDT conjugated polymers.

2.2 Optical and electrochemical properties

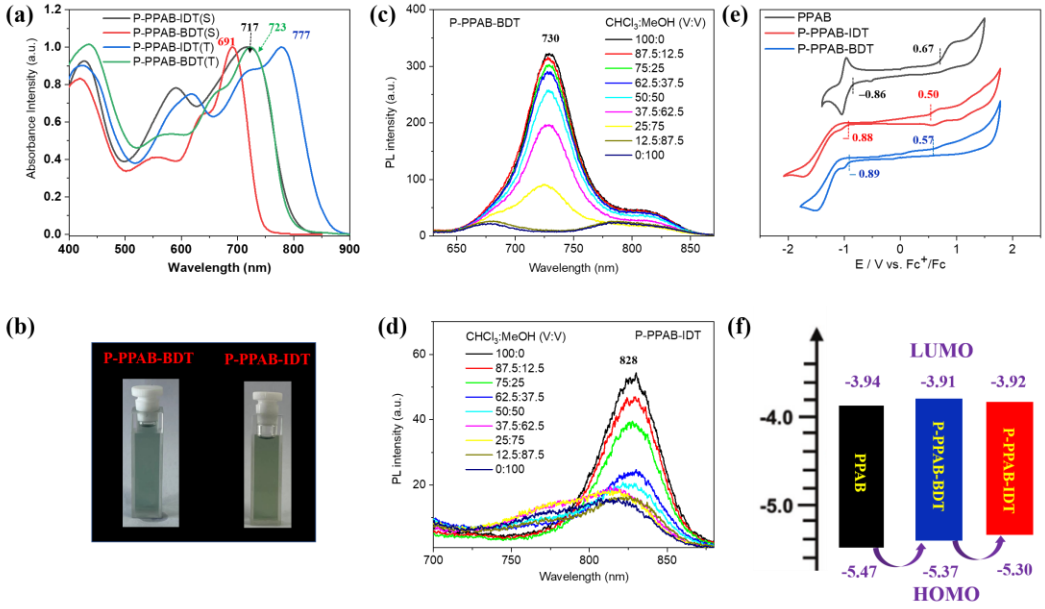

Figure 1. (a) UV/vis absorption spectra of P-PPAB-IDT and P-PPAB-BDT conjugated polymers in chloroform solution (S) and thin film (T). (b) Photos of the two polymers in chloroform solution. Photoluminescence (PL) spectra of (c) P-PPAB-BDT and (d) P-

PPAB-IDT polymers in mixture solvent of chloroform ($CHCl_3$) and methanol (MeOH) upon various volume ratios ($CHCl_3$:MeOH, V:V), excited at 600 nm. (e) Cyclic voltammograms of the PPAB monomer and the polymers-based thin films deposited on ITO substrates. Electrolyte: 0.1 M $TBAPF_6$ in acetonitrile. Potential calculated versus ferrocene. Scan rate: 100 mV s^{-1}; T = 25 °C. (f) Energy diagram of the PPAB monomer and the polymers. The electrochemical properties of both polymers were investigated by cyclic voltammetry (CV). The HOMO and LUMO energy levels were calculated based on the oxidation and reduction onset potentials (i.e., $E_{ox\ onset}$ and $E_{red\ onset}$), and the empirical equations: $E(HOMO) = -e\ [E_{ox\ onset} - E_{1/2(ferrocene)} + 4.8]$ eV and $E\ (LUMO) = -e\ [E_{red\ onset} - E_{1/2(ferrocene)} + 4.8]$ eV.

To evaluate the possible aggregation of the polymer film, the optical properties of the polymers were characterized. Figures 1a and S2 compare the absorption spectra of PPAB monomer with that of P-PPAB-IDT and P-PPAB-BDT polymers in chloroform solution (S) and thin film (T). The related optical parameters are summarized in Table S1. The PPAB solution exhibits a blue color. The absorption spectrum of the PPAB monomer in chloroform shows a distinct absorption maximum ($\lambda_{abs.max}$) at 664 nm with an extinction coefficient of 2.3×10^4 L mol^{-1} cm^{-1}, with a blue-shift around 37 nm compared to the case of its thin film ($\lambda_{abs.max}$ = 701nm). After the polymerization, the

absorption spectra of both polymers present a large shift towards the longer wavelength in solution compared to that of PPAB monomer (from 664 to 717 nm and from 664 to 691 nm for P-PPAB-IDT and P-PPAB-BDT, respectively). The red-shift could be ascribed to the π-conjugation skeleton extension as well as to the donor-acceptor interaction within the polymer backbones, which inevitably cause the ICT process to generate more delocalized intramolecular π-orbitals and, thus, to efficiently increase the conjugation lengths.[35] Regarding the polymer films, clearly red-shifted absorption spectra are also observed compared to their solution counterparts (Figure 1a). This red-shift could be, in turn, attributed to the aggregation and closer packing of the polymer backbone in solid-state rather than in solution, since in the latter case the polymer chains are likely in the form of a single (macro)-molecular state.[36] P-PPAB-BDT shows a small bathochromic shift of only 31 nm, while P-PPAB-IDT exhibits a ~60 nm red-shift. The larger red-shift observed in the absorption spectrum of P-PPAB-IDT polymer film indicates the stronger aggregation and/or closer packing for the IDT-based polymer film compared to the case of the BDT-based polymer. P-PPAB-BDT also possesses a broad absorption band ranging from 500 nm to 800 nm, while the long absorption tail of the IDT-based polymer film extends up to 850 nm. This further suggests that efficient molecular packing occurs in the case of P-PPAB-IDT thin film, which assists the efficient charge transport between the adjacent polymers.[37-40] In addition, the broad

optical absorption of PPAB-based polymers may suggest that these sorts of copolymers could be good candidates as light absorbers for other optoelectronic applications, such as solar cells and photodetectors. The optical band gaps were also calculated from the absorption onsets, and they are included in Table S1.

We then in turn measured the steady-state photoluminescence (PL) spectra for two polymers both in film and in solution phases by exciting the samples at 600 nm. For the film case, there was surprisingly no observed emission signal (data is not shown here) for both polymers, possibly due to the strong quenching effect induced by the aggregation within the polymer film.[41-42] In contrast, this PL self-quenching effect can be sufficiently reduced or eliminated by dissolving the polymer (with a constant concentration of 1×10^{-3} mg/mL) in a mixture solvent of chloroform ($CHCl_3$) and methanol (MeOH) with various volume ratios (see the details for sample preparation in the Supporting Information), which PL spectra are shown in Figure 1c for P-PPAB-BDT and in Figure 1d for P-PPAB-IDT, respectively. [43] For the P-PPAB-BDT solution, with the increase in the amount of $CHCl_3$ in the mixture solvent, the intensity of the dominant PL peak at 730 nm is clearly enhanced, which exhibits a reasonable Stokes-shift of ~39 nm compared to its first exciton peak at 691 nm (see Figure 1a). On the other hand, the PL spectra of the P-PPAB-IDT solution demonstrate a similar behavior upon the $CHCl_3$ amount dependence in the mixture solvent, however the absolute

intensity is much weak which is nearly six times lower than those of P-PPAB-BDT case. Moreover, an extremely big Stokes-shift of ~111 nm is observed by comparing the PL peak at 828 nm with its corresponding first exciton peak at 717 nm for P-PPAB-IDT solution (see Figure 1a), suggesting that there coule be plenty of defects or traps within the P-PPAB-IDT polymer which can effectively quench the PL in the form of non-radiative recombination.

The electrochemical properties of the polymers were further investigated by cyclic voltammetry (CV). The experimental details are described in the SI. Based on the onset reduction and oxidation potentials, the LUMO/HOMO energy levels of the monomer and polymers can be estimated. In Figure 1e, the PPAB monomer shows reversible cathodic and anodic waves. The onset oxidation and reduction positions occur at 0.67 and -0.86 V, respectively, according to which the HOMO and LUMO energy levels were calculated as -5.47 eV and -3.94 eV. In the case of the polymers, both onsets of oxidation and reduction turn up at lower potentials compared to the corresponding potentials of PPAB monomer. The polymers demonstrate similar LUMO energy levels (-3.92 eV for P-PPAB-IDT and -3.93 eV for P-PPAB-BDT). The electron-withdrawing units contribute more to the alignment of the LUMO energy levels of the corresponding D-A typed polymers, while the electron-rich moieties are in turn crucial for modulating the HOMO energy levels. The similar LUMO energy levels of the two polymers might

be due to the fact that the acceptors of the polymer backbone are identical, which can render the electron injection from the electrode to the semiconductor layer comparable when they are employed in optoelectrical transistor applications. On the other hand, the anodic oxidation potentials of the polymers at 0.50 V (P-PPAB-IDT) and 0.57 V (P-PPAB-BDT) were used to estimate the HOMO energy levels as -5.30 eV and -5.37 eV for P-PPAB-IDT and P-PPAB-BDT, respectively. Due to the low HOMO energy levels of the polymers, a good hole injection could be expected in the performance of OFET devices.[38] The polymers feature quite narrow HOMO-LUMO band gaps of 1.38 eV (P-PPAB-IDT) and 1.46 eV (P-PPAB-BDT), which are smaller than that (1.53 eV) of PPAB monomer. It is noted that the electrochemical band gaps are generally larger than the optical ones, mainly due to the interfacial barrier for the charge injection during the CV experiment.

2.3 Thin film structures and morphologies

For polymer-based OFETs, charge transport only occurs between several neighboring molecule layers. Thus, the polymer packing, as well as the thin film morphology, can significantly influence the field-effect performance of the transistors. The structures of the polymer thin films were accordingly characterized by X-ray diffraction (XRD) measurements. The experimental details are described in the SI. Figure 2 compares the XRD patterns of the polymer films spin-coated on the SiO_2/Si

substrate. The XRD patterns of both films show primary diffraction peaks at $2\theta = 5.39^{o}$ and 6.58^{o} for P-PPAB-BDT and P-PPAB-IDT, respectively, which correspond to the inter-lamellar distances of 1.638 nm and 1.342 nm. The peaks at around 20.2^{o} for both polymers originate from the co-facial π-π stacking with a *d*-spacing distance of 0.439 nm. The diffraction peak of P-PPAB-IDT is slightly sharper than that of P-PPAB-BDT, implying the formation of longer-range ordering for the former case.

The optical microscope images (Figures 2b and 2c) demonstrate well-distributed, smooth, and flat surfaces for two conjugated polymer films, indicating superior film-forming capabilities achieved in both cases. Similar results can be also drawn from the AFM surface phase images of the polymer films. Nevertheless, a significant morphological difference is observed from the AFM images (Figures 2d and 2e) of two polymer films. The BDT-based polymer film presents a remarkably disordered state with inferior crystallinity. On the contrary, the IDT-based polymer film rather possesses larger and well-interconnected crystalline grains at the scale bar compared to the BDT-based film. This observation is consistent with the XRD data. It is well known that the high crystallinity is favorable for the charge carrier mobility, thereby improving the charge transport, as expected in the case of IDT-based polymer.[44]

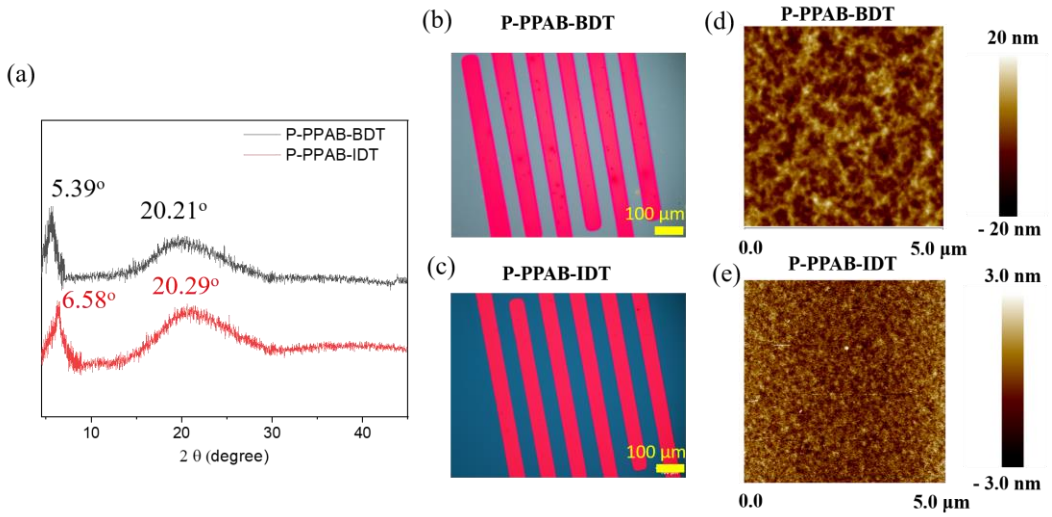

Figure 2. (a) Transmission XRD diagrams of the polymer films. (b,c) Conventional optical images of the polymer films deposited on the OFET devices prepared by spin-coating. (d,e) AFM images of the P-PPAB-BDT film (d, size 5 × 5 μm) and the P-PPAB-IDT film (e, size 5 × 5 μm).

2.4 Quantum chemical computation

To gain insights into the polymer backbone configuration, the frontier molecular orbital feature and the HOMO/LUMO energy levels of P-PPAB-BDT and P-PPAB-IDT were computationally simulated via density functional theory (DFT) calculations. Typically, the DFT calculations at the B3LYP/6-31G* level of theory were performed by using the model compound containing dimers with the long alkoxyl groups replaced by methoxy groups. As shown in Figure 3a, the electronic cloud distribution at the HOMO levels for both polymers is quite similar, indicating the delocalization on the polymer backbone, however their LUMO orbitals are clearly different. The P-PPAB-BDT

polymer exhibits PPAB-dominant LUMO distribution with some electron delocalization along with the conjugation backbone, whereas the electron distribution of the LUMO for P-PPAB-IDT is located only at the electron-withdrawing PPAB groups. This suggests that P-PPAB-IDT has stronger ICT effect compared to P-PPAB-BDT, which means that the BDT-based polymer is more localized. The theoretical HOMO/LUMO energy levels were calculated as -2.83/-4.56 eV and -2.85/-4.74 eV for P-PPAB-IDT and P-PPAB-BDT, respectively. The P-PPAB-IDT polymer shows a higher HOMO energy level and a smaller band gap than those of the P-PPAB-BDT, which is in good agreement with the previous electrochemical analysis. The calculated band gap values are larger than the electrochemical ones, likely due to the fact that the calculation results are restricted to the single molecule with two repeating units regardless of the interaction between the individual molecules.[24] Figure 3b shows that all the twisting angles between the aromatic units within the backbone of the P-PPAB-IDT dimer are smaller than those of P-PPAB-BDT dimer, when accounting for the dihedral angles between donor groups and acceptor groups. This clearly implies that the polymer backbone of P-PPAB-IDT possesses higher coplanarity than the case of P-PPAB-BDT, which is profitable for the molecular packing, as supported by their optical properties.

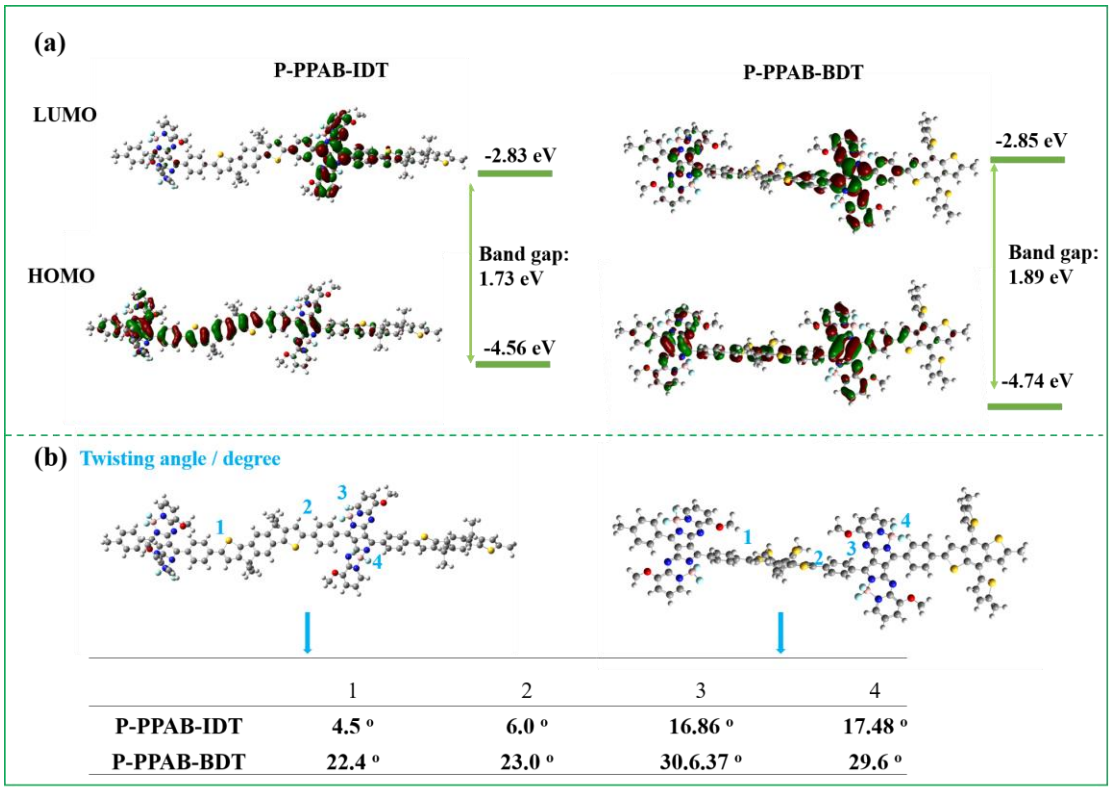

	1	2	3	4
P-PPAB-IDT	**4.5 °**	**6.0 °**	**16.86 °**	**17.48 °**
P-PPAB-BDT	**22.4 °**	**23.0 °**	**30.6.37 °**	**29.6 °**

Figure 3. Computational calculations of the simplified dimers of both polymers obtained at the B3LYP/6-31G* level. (a) Molecular orbital surfaces of the HOMO and LUMO energy levels and the band gaps of two polymers. (b) Chemical structures of the simplified dimers highlighted with the twisting angles.

2.5 Photosensing performance of the field-effect transistors

In order to evaluate the optoelectrical characteristics of P-PPAB-IDT and P-PPAB-BDT conjugated polymers, we fabricated organic phototransistors with a bottom-gate bottom-contact (BGBC) configuration (see the device schematic in Figure 4a). Highly doped silicon (Si) and SiO_2 were employed as the gate electrode and gate dielectric, respectively. The source and drain electrodes were vacuum-deposited on an

octadecyltrichlorosilane-treated Si/SiO_2 substrate as an Au layer (30 nm thickness) through a shadow mask, followed by the direct deposition of the polymer solution in toluene. The devices were then treated upon the thermal annealing at 180 ºC for 10 min in a nitrogen-filled glove box, aiming to remove the solvent residues and thus to obtain high-quality polymer films. The IDT-based phototransistors demonstrate typical p-type transfer characteristic curves with a high I_{on}/I_{off} ratio of approximately 10^3 (Figure 4b). In addition, the average charge carrier mobility (μ_h) of this polymer could reach 0.023 $cm^2\ V^{-1}\ s^{-1}$ (highest value of 0.026 $cm^2\ V^{-1}\ s^{-1}$), and the threshold voltage (V_{th}) is approximately -23 V extracted from 8 devices. As a comparison, the BDT-based phototransistors show ambipolar transfer characteristic curves with hole/electron mobilities (μ_h/μ_e) of $10^{-3}/10^{-4}$ $cm^2\ V^{-1}\ s^{-1}$, which are much lower than that of IDT-based phototransistors (Figure 4 and Table S2). As previously stated, the charge mobility difference is mainly attributed to the improved ICT effect and higher planarity of the backbone in the case of P-PPAB-IDT, compared to the BDT polymer. In addition, the observed strong aggregation and a high degree of crystallinity in P-PPAB-IDT film are also advantageous for the charge transport between the neighboring molecules.[38,45]

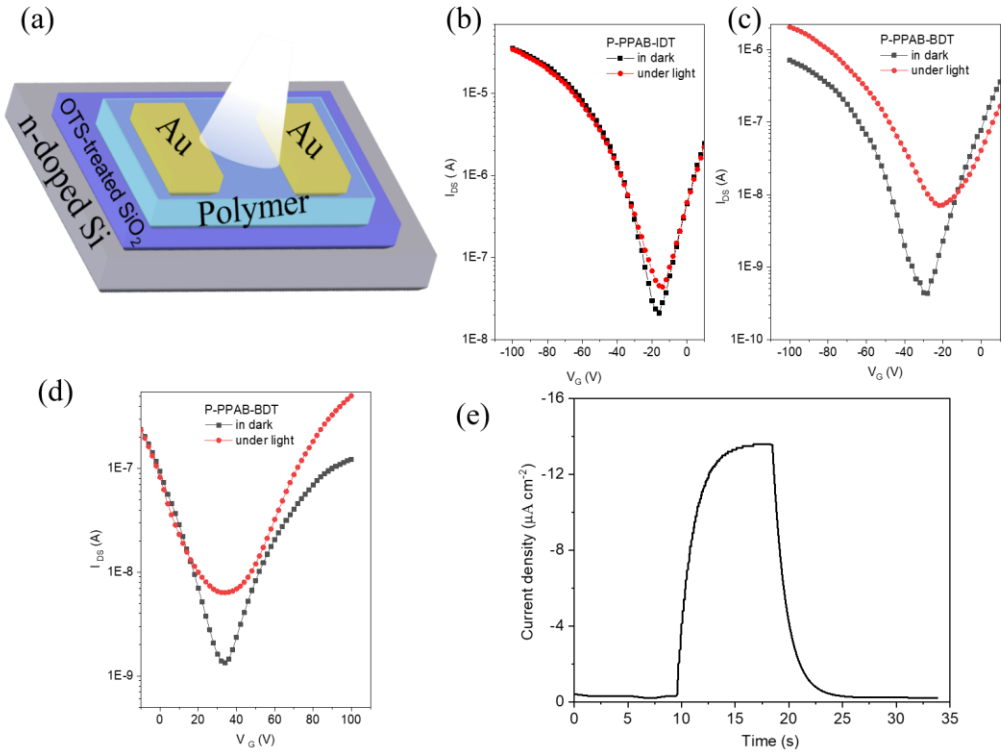

Figure 4. (a) Schematic illustration of organic phototransistors with IDT or BDT-based polymer as the active and photosensitive layer. (b) Photoswitching characteristic curves of IDT-based phototransistors in dark and under the white light illumination (Ee = 0.27 mW cm^{-2}). (c,d) Photoswitching characteristic curves of BDT-based phototransistors in dark and under the white light illumination (Ee = 0.27 mW cm^{-2}) in the p-type sweeping area (c) and n-type sweeping area (d). (e) Transient photocurrent profile of the BDT-based phototransistor under white light illumination (0.27 mW cm^{-2}) and a bias of -10 V.

It has been widely reported that the high charge carrier mobility is positive for the

enhanced photosensing performance of the phototransistors. However, a surprising phenomenon has been observed in this work, as the organic phototransistors based on P-PPAB-IDT polymer with high charge mobility show no photoresponse to the white light illumination, whereas the ones based on P-PPAB-BDT polymer with low charge mobility present a significant photoresponse to the same light source. As observed in Figures 4c and 4d, upon the illumination with an incident light intensity of 0.27 mW cm^{-2}, the I_{off} of the organic phototransistors clearly increases, approximately in average 21.6 and 5.2 in the p-type and n-type sweeping areas, respectively (Figure S3). This is plausibly attributed to the fact that the generation of photoinduced charge carriers increases the intrinsic charge carrier density in the active layer, and the polymer π-π stacking and aggregation may also accelerate the recombination and quenching of photogenerated holes and electrons. This speculation can be also supported by the previous PL data that P-PPAB-IDT polymer possesses strong PL self-quenching ability, leading to inherently low density of photogenerated charge carriers partially responsible for the low or negligible photoresponse.

To gain further insights into the understanding of the distinct photoresponse provided only by BDT-based phototransistors, we measured the transient photocurrent profile of the best BDT-based phototransistor under white light illumination while applying a constant bias of -10 V, as shown in Figure 4e. The transient photocurrent

profile exhibits a time-dependent growth and a decay behavior for an exposure time of 8 s to the white light (0.27 mW cm^{-2}). The BDT-based device requires about 3.2 s to rise to 90% of the photocurrent saturation value in the growing edge and 6.9 s to decay to the end in the falling edge. Such long response times in the order of several seconds are likely ascribed to the dispersive diffusion of the photogenerated charge carriers, which has also been observed for other types of polymer-based phototransistors.[46] It is noteworthy that the holes can be effectively localized at the HOMO/LUMO level of the P-PPAB-BDT polymer (see the DFT simulation results in Figure 3), while the electrons can drift to the collection electrodes upon the effect of the applied bias. This sort of strong charge transport unbalance indeed induces a photoconductive gain, [47,48] leading to the efficient photocurrent generation and dissociation detected in the case of BDT-based phototransistors, which has not been observed for IDT-based devices. Such results authenticate that our novel synthetic strategy for the synthesis of the P-PPAB-BDT polymer could provide significant hints for the fabrication of high-photosensitivity conjugated polymers in organic phototransistors by effectively reducing the π-π packing and aggregation.

3. Conclusions

Traditionally, the photosensitivity of polymer semiconductors is highly dependent

on their charge carrier mobilities. However, high charge mobility is typically induced by the high polymer π-π packing and aggregation, which are, in turn, detrimental to an increase in photosensitivity. Therefore, in this work, we aimed at exploring the influence of charge carrier mobility and π-π packing on the photoswitching characteristics of the phototransistors. Two novel D-A conjugated polymers (PPAB as the electron-withdrawing unit and IDT or BDT as the electron-rich unit) were synthesized through the Stille-coupling polymerization. The P-PPAB-IDT polymer shows a much higher charge carrier mobility (up to 0.02 $cm^2 V^{-1} s^{-1}$) than P-PPAB-BDT polymer ($\mu_h=10^{-3}$ $cm^2 V^{-1} s^{-1}$; $\mu_e=10^{-4}$ $cm^2 V^{-1} s^{-1}$) due to the better planarity, larger π-π conjugated structures, and higher crystallinity of P-PPAB-IDT. Interestingly, P-PPAB-BDT exhibits a distinct photoresponse to white light illumination with average I_{light}/I_{dark} ratios of 21.6 in the p-type area and of 5.2 in the n-type area, while P-PPAB-IDT does not display any response to white light. This is plausibly attributed to the fact that the generation of photoinduced charge carriers increases the intrinsic charge carrier density in the active layer, and the polymer π-π stacking and aggregation may also accelerate the recombination and quenching of photogenerated holes and electrons.

This work offers an effective approach for the design, synthesis, and optoelectronic application of high-photosensitivity conjugated polymers by reducing the π-π packing and aggregation. Moreover, the PPAB units might be favorable for other

applications as dyes and colorants, and the co-monomer electron-withdrawing units could be used in photovoltaics or phototransistors by leveraging their wide and strong absorption in the visible range. More studies on PPAB-based polymers regarding phototransistors of field-effect transistors are currently being investigated in our group.

Conflicts of interest

The authors declare no competing financial interest.

Acknowledgements

The authors acknowledge the support from Natural Science Foundation of China, under Grant 21805151, Young Taishan Scholars under Grant 201909120, Science foundation for postdoctoral research of Shandong. M.L. thanks the Finnish Cultural Foundation (No. 00220107) for funding. P.V. acknowledges the financial support of Jane and Aatos Erkko foundation (SOL-TECH project). This work is part of the Academy of Finland Flagship Programme, Photonics Research and Innovation (PREIN), Decision No. 320165.

References

[1] T. Pal, M. Arif, S. I. Khondaker, *Nanotechnology*, **2010**, 325201.

[2] P. Gu, Y. Yao, L. Feng, S, Niu, *Polym. Chem*., **2015**, *6*, 7933.

[3] G. Chaji, A, Nathan, Q, Pankhurst, *Appl. Phys. Lett*., **2008**, *20*, 203504.

[4] Y. Moon, C. Lee, H. Kim, J. Park, Y. Kim, *Polym. Chem*., **2019**, *10*, 6324.

[5] X. Huang, D. Ji, H. Fuchs, W. Hu, T. Li, *ChemPhotoChem*, **2020**, *4*, 9.

[6] Y. S. Rim, Y. M. Yang, S. H. Bae, H. Chen, C. Li, M. S. Goorsky, Y. Yang, *Adv. Mater*., **2015**, *27*, 6885.

[7] X. Liu, L. Tavares, A. Osadnik, J. Lausen, j. Kongsted, A. Lutzen, H. Rubahn, J, Kijelstrup-Hansen, *Org. Electron*., **2014**, *15*, 1273.

[8] K.-J. Baeg, D. Khim, J. Kim, B.-D. Yang, M. Kang, S.-W. Jung, I.-K. You, D.-Y. Kim, Y.-Y. Noh, *Adv. Funct. Mater*., **2012**, *22*, 2915.

[9] P. C. Y. Chow, N. Matsuhisa, P. Zalar, M. Koizumi, K. Yokota, T. Someya, *Nature Commun.,* **2018**, *9*, 4546.

[10] T. Leydeker, M. Herder, E. Pavlica, G. Bratina, S. Hecht, E. Orgiu, P. Samori, *Nat. Nanotechnol*., **2016**, *87*.

[11] H. Hwang, H. Kim, S. Nam, D. Bradley, C. Ha, Y. Kim, *Nanoscale*, **2011**, *3*, 2275.

[12] H. Han, S. Nam, J. Seo, J. Jeong, H. Kim, D. Bradley, Y. Kim, *IEEE J. Sel. Top. Quantum Electron*., **2016**, *22*, 147.

[13] Y. Liu, H. Wang, H. Dong, L. Jiang, W. Hu, X. Zhan, *Small*, **2012**, *9*, 294.

[14] H. Dong, H. Zhu, Q. Meng, X. Gong, W. Hu, *Chem. Soc. Rev.*, **2012**, *41*, 1754.

[15] C. Wang, H. Dong, W. Hu, Y. Liu, D. Zhu, *Chem. Rev.*, **2012**, *112*, 2208.

[16] H. Zhang, K. Yang, K, Zhang, Z. Zhang, Q. Sun,W. Yang, *Polym. Chem*., 2018, *9*, 1807.

[17] F. Lin, S. Lin, C. Chin, W. Chuang, C. Hsu, *Polym. Chem*., **2018**, *9*, 28.

[18] Y. Liu, H. Dong, S. Jiang, G. Zhao, Q. Shi, J.Tan, L. Jiang, W. Hu, X. Zhan, *Chem. Mater.*, **2013**, *25*, 2649.

[19] G. L. Gibson, T. M. Mccormic, D. S. Seferos, *J. Am. Chem. Soc.*, **2012**, *134*, 539.

[20] P. M. Beaujuge, J. M. J. Frechet, *J. Am. Chem. Soc*., **2011**, *133*, 20009.

[21] S. Nam, J. Seo, H. Han, H. Kim, D. Bradley, Y. Kim, *ACS Appl. Mater. Interfaces*, **2017**, *9,* 14983.

[22] P.-L. T. Boudreault, A. Najari, M. Leclerc, *Chem. Mater.*, **2011**, *23*, 456-469.

[23] W. W. Bao, R. Li, Z. C. Dai, J. Tang, J. Hua, *Front. Chem.*, **2020**, *8*, 679.

[24] H. Zhang, R. Li, Z. Deng, S. Cui, Y. Wang, M. Zheng, W. Yang, *Dyes and Pigments*, **2020**, *181*, 108552.

[25] J. Yao, C. Yu, Z. Liu, H. Luo, Y. Y, G. Zhang, D. Zhang, *J. Am. Chem. Soc.*, **2016**, *138*, 173.

[26] M. J. Cho, J. S, T. R. Hong, H. A. Um, T. W. Lee, G. W. Kim, J. H. Kwon, D. H. Choi, *Polym. Chem.*, **2015**, *6*, 150.

[27] V. D. Mitchell, D. J. Jones, *Polym. Chem.*, **2018**, *9*, 795.

[28] K. Zhang, B. Tieke, F. Vilela, PJ, Skabara, *Macromol. Rapid. Commun*., **2011**, *32*,

825.

[29] I, Welterlich, J.-M. Neudorfl, B. Tieke, *Polym. Chem*., 2015, *6*, 1005.

[30] S. Wiktorowski, C. Rosazza, M. J. Winterhalder, E. Daltrozzo, A. Zumbusch, *Chem. Commun.*, **2014**, *50*, 4755.

[31] Y. Kage, S. Mori, M. Ide, A. Saeki, H. Furuta, S. Shimizu, *Mater. Chem. Front.*, **2018**, *2*, 112.

[32] M. Poddar, G. Sivakumar, R. Misra, *J. Mater. Chem. C*, **2019**, *7*, 14798.

[33] P. Thamaraiselvi, E. Varathan, V. Subramanian, S. Easwaramoorthi, *Dyes and Pigments*, **2020**, *172,* 107838.

[34] H. Zhang, M. Liu, W. Yang, L. Judin, T. I. Hukka, A. Priimagi, Z. Deng, P. Vivo, *Adv. Mater. Interfaces*, **2019***, 6*, 1901036.

[35] H. Zhang, S. Ying, J. Zhang, B. Tieke, W. Yang, *Polymer*, **2015**, *60*, 215.

[36] R. Li, Z. Dai, M. Zheng, C. Wang, Z. Deng, T. Zhuang, K. Feng, W. Yang, K. Yang, H. Zhang, *Macromol. Rapid. Commun*., **2021**, *42*, 2000703.

[37] X. Guo, A. Facchetti, T. J. Marks, *Chem. Rev.*, **2014**, *114*, 8943.

[38] T. Mikie, I. Osaka, *J. Mater. Chem. C*, **2020**, *8*, 14262.

[39] Y. Wang, L. Sun, C. Wang, F. Yang, X. Ren, X. Zhang, H. Dong, W. Hu, *Chem. Soc. Rev*., **2019**, *48,* 1492.

[40] L. Shi, Y.Guo, W. Hu, Y. Liu, Mater. *Chem. Front.*, **2017**, *1*, 2423.

[41] X. Ma, R. Sun, J. Cheng, J. Liu, F. Gou, H. Xiang, X. Zhou, *J. Chem. Educ.*, **2016**, *93*, 345–350.

[42] Y. Huang, J. Xing, Q. Gong, L-C. Chen, G. Liu, C. Yao, Z. Wang, H-L. Zhang, Z. Chen, Q. Zhang, *Nature Commun*, **2019**, *10*, 169.

[43] D. G. Congrave, B. H. Drummond, V. Gray, *Polym. Chem*., **2021**, *12*, 1830.

[44] Z. Deng, X. Hao, P. Zhang, L. Li, X. Yuan, T. Ai, W. Bao, K. Kou, *Dyes and Pigments*, **2019**, *162*, 883.

[45] W. Wu, Y. Liu, D. Zhu, *Chem. Soc. Rev*., **2010**, *39*, 1489.

[46] L. Caranzi, G. Pace, M. Sassi, L. Beverina, M. Caironi, ACS Appl. Mater. Interfaces, **2017**, *9*, 34, 28785.

[47] L. Li, F. Zhang, J. Wang, Q. An, Q. Sun, W. Wang, J. Zhang, F. Teng, *Sci. Rep*., **2015**, *5*, 9181.

[48] M. Hiramoto, T. Imahigashi, M. Yokoyama, *Appl. Phys. Lett*., **1994**, *64*, 187.

Supporting information

From transistors to phototransistors by tailoring the polymer stacking

Shuaiwei Cui,[a] Dongxu Liang,[a] Maning Liu,[b] Paola Vivo,[b] Meng Zheng,[a] Tao Zhuang,[a] Qikun Sun,[a] Wenjun Yang,[a] Haichang Zhang[a]*

[a]Key Laboratory of Rubber-Plastics of Ministry of Education/Shandong Province (QUST), School of Polymer Science & Engineering, Qingdao University of Science & Technology, 53-Zhengzhou Road, Qingdao, 266042, PR China

[b]Hybrid Solar Cells, Faculty of Engineering and Natural Sciences, Tampere University, P.O. Box 541, Tampere FI-33014, Finland

Corresponding author: Haichang Zhang: haichangzhang@hotmail.com

Contents

1. Experimental Procedures

1.1 Materials

All reagents were purchased from commercial sources and used without further purification unless otherwise noted. Tetrakis(triphenyl-phosphine)palladium(0) ($Pd(PPh_3)_4$), anhydrous magnesium sulfate and anhydrous toluene were distilled over sodium and freshly used. Nitrogen (N_2) protection was used for all oxygen and moisture-sensitive reactions. The starting PPAB monomer was synthesized according to the literatures.[1]

1.2 Synthesis of polymers

Precursor (1): 2-Amino-3-(2-hexyldecyloxy)pyridine

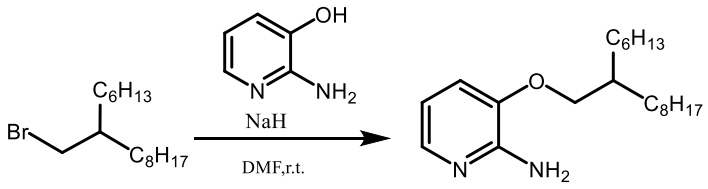

Scheme 1. Synthetic route of precursor (1).[1]

In a 500 mL flask, 2-amino-3-hydroxypyridine (2.64 g, 24 mmol) and activated sodium hydride (1.40 g, 58 mmol) was stirred in a dry DMF solution (180 mL) under room temperature for 2h at N_2 atmosphere protection. Subsequently, a solution of 7-(bromomethyl)pentadecane (10.69 g, 35 mmol) in dry DMF solution (10 mL) was added. The reaction mixture stirred another 30 h in dark, and then was poured in water, extracted with chloroform. The crude product was purified using the column chromatography firstly by pure hexane as an eluent to remove residual DMF, and subsequently using methanol as an eluent to obtain dark brown oil product (3.82 g, yield: 47.6 %). ^{1}H NMR ($CDCl_3$, 500 MHz, 295K): [ppm] = 7.60 (d, J = 5.3 Hz, 1H), 6.86 (d, J = 8.3 Hz, 1H), 6.56 (dd, J_1 = 7.9vHz, J_2 = 4.9 Hz, 1H), 4.75 (br, 2H), 3.82 (d, J = 5.3 Hz, 2H), 1.82-1.74 (m, 1H), 1.46-1.14 (m, 24H), 0.90-0.78 (m, 6H)；^{13}C

NMR ($CDCl_3$, 125 MHz, 295K): [ppm] = 150.28, 141.99, 138.20, 115.30, 113.49, 70.84, 64.90, 53.40, 45.93, 36.85, 35.10, 32.32, 31.88, 31.82, 31.47, 29.98, 29.65, 29.56, 29.14, 22.65, 14.08.

Precursor (2):

3,6-Bis(4-bromophenyl)-2,5-dihydropyrrolo[3,4-c]pyrrole-1,4-dione (DPP)

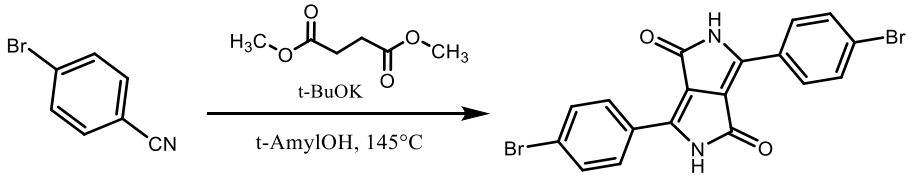

Scheme 2. Synthetic route of precursor (2).

In a 250 mL flask, passium tert-butanolate (11.5 g, 102.5 mmol) and 4-bromobenzonitrile (18.2g, 100mmol) were added to the t-amyl alcohol solution (180 mL) at 110 ºC under N_2 atmosphere. After the mixture was fully dissolved and stirred for about 2 h, a solution of diethyl succinate (6.64 mL, 50 mmol) in t-amyl alcohol was added dropwise for another 1 h. Subsequently, the mixture was heated to 140 ℃ for another 5 h. After that acetic acid and methanol were added. The precipitated solids were filtered and washed with water and methanol several times and dried at 80 °C in vacuum, affording a red powder product (12.3 g, yield: 55.1 %). The product was used for the next step without further characterization due to the pigment's poor solubility.

PPAB:

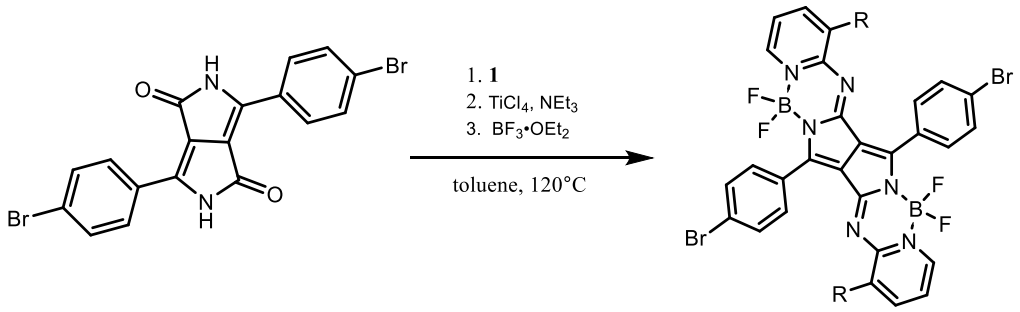

Scheme 3. Synthetic route of PPAB.

In a 250 mL flask, 1 (3.0 g, 9.0 mmol) and 2 (0.89 g, 2.0 mmol) were added in a dry toluene solution (180 mL) at room temperature. Subsequently, the temperature of the mixture was heated to 110 ℃ and stirred for 40 min. Then titanium tetrachloride (1.5 ml, 13.5 mmol) was added to the mixture. After 5 minutes triethylamine (5.0 mL, 35 mmol) was added. When formation of imine was confirmed by TLC analysis after 2 hours, borontrifluoride etherate (4.5 ml, 36.5 mmol) was added. The mixture was poured to water and extracted with dichloromethane after it was refluxed for another 16 h. The organic layers were dried on sodium sulfate and concentrated in vacuo to provide blue solids. The crude compound was purified on silica gel column using dichloromethane as eluent to obtain blue solids (0.655 g, Yield: 28%). ^{1}H NMR (500 MHz, $CDCl_3$, 295 K): [ppm] = 8.33 (d, J = 9.5 Hz, 4H), 7.85 (d, J = 6.0 Hz, 2H), 7.63 (d, J = 8.5Hz, 4H), 7.23 (d, J = 9.5 Hz, 2H), 7.04 (dd, J = 6.0 Hz, J = 8.0 Hz 2H)，1.48-1.16 (m, 48H), 0.90-0.78 (m, 12H). ^{13}C NMR ($CDCl_3$, 125 MHz, 295 K): [ppm] = 151.76, 150.15, 149.44, 145.40, 131.28, 130.18, 128.41, 127.71, 126.86, 124.87, 119.74, 119.38, 116.84, 71.58, 36.92, 30.87, 30.79, 29.86, 28.99, 28.66, 28.52, 25.44, 21.63, 13.04. MS (MALDI-TOF) m/z: calculated for $C_{60}H_8B_2Br_2O_2F_4$ 1172.48; found: 1171.50 [M^-]. Extinction coefficient at 691 nm = 2.3×10^4 L mol^{-1} cm^{-1}.

Polymer P-PPAB-IDT

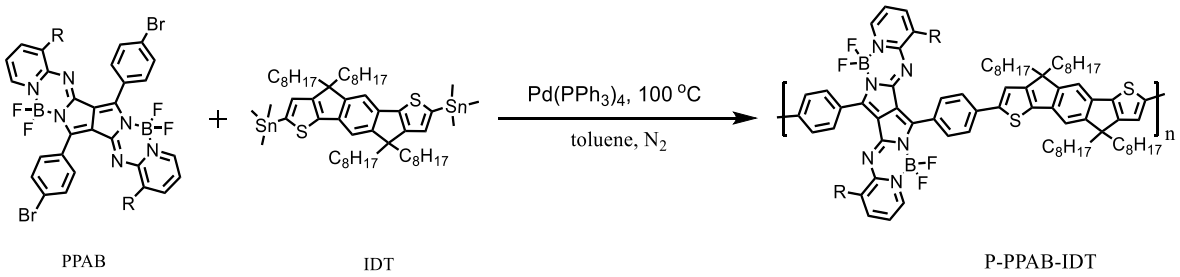

Scheme 4. Synthetic route of P-PPAB-IDT polymer.

In a 50 mL flask, PPAB (176 mg, 0.15mmol) and IDT (157 mg, 0.15mmol) were stirred in toluene at room temperature under N_2 about 10 min. Subsequently, palladium tetraphenylphosphate (3.5 mg, 0.003mmol) was added to the reaction mixture under N_2 protection. The mixture was stirred for 36 h at 90 °C. After cooling, the dark solution was diluted with DCM (50 ml)) and extracted with brine (2×50 ml) and water (50 ml). The organic phase was dried with $MgSO_4$, and the solvent was evaporated. The polymer was dissolved again in DCM and precipitated with methanol giving a dark solid The product was purified by Soxhlet extraction with methanol, n-hexane, and THF to remove the oligomers and impurities. Finally, it was washed with chloroform to collect the product P-PPAB-IDT (142 mg, yield: 54.8 %). Molecular weight (GPC, $CHCl_3$): Mw = 16.0 KDa, PDI = 2.5. ^{1}H-NMR (500 MHz, $CDCl_3$) δ ppm: 8.563 (s, 4H), 7.83-8.09(d, 6H), 7.37-7.47 (d, 2H), 7.30-7.35 (br, 2H), 6.95-7.09 (br, 4H), 3.96 (s, 4H), 2.91 (s, 4H), 1.97 (s, 2H), 1.31-1.47 (br, 96H), 0.83-0.96 (m, 24H).

Polymer P-PPAB-BDT:

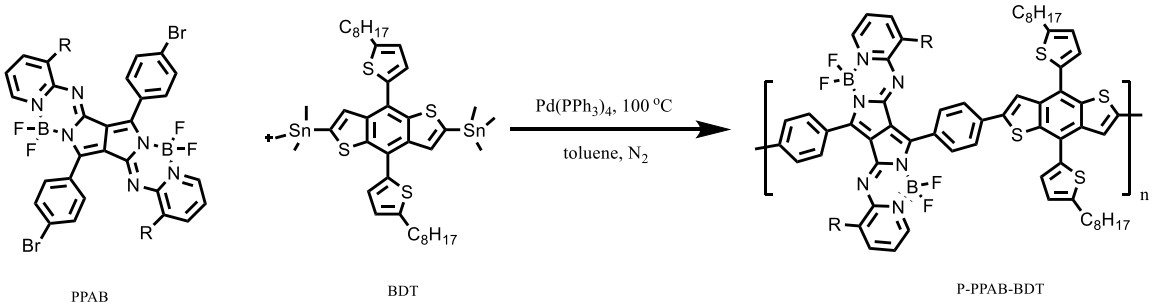

Scheme 5. Synthetic route of P-PPAB-BDT polymer.

In a 50 mL flask, PPAB (176 mg, 0.15mmol) and BDT (136 mg, 0.15mmol) were stirred in toluene at room temperature under N_2 for about 10 min. Subsequently, palladium tetraphenylphosphate (3.5 mg, 0.003mmol) was added to the reaction mixture under N_2 protection. The mixture was stirred for 36 h at 90 °C. After cooling, the dark solution was diluted with DCM (50 ml)) and extracted with brine (2×50 ml) and water (50 ml). The organic phase was dried with $MgSO_4$, and the solvent was evaporated. The polymer was dissolved again in DCM and precipitated with methanol giving a dark solid The product was purified by Soxhlet extraction with methanol, n-hexane, and THF to remove the oligomers and impurities. Finally, it was washed with chloroform to collect the product P-PPAB-BDT (141 mg, yield: 59 %). Molecular weight (GPC, $CHCl_3$): Mw = 19.3 KDa, PDI = 2.8. ^{1}H-NMR (500 MHz, $CDCl_3$) δ ppm: 8.51-8.62 (br, 4H), 7.83-8.09(m, 6H), 7.41-7.39 (d, 2H), 7.18-7.22 (br, 2H), 6.90-7.05 (d, 4H), 3.86 (s, 4H), 2.86 (s, 4H), 1.78 (s, 2H), 1.31-1.47 (br, 24H), 1.02-1.21 (br, 48H), 0.76-0.99 (m, 18H).

1.3 Characterization for polymers

1.3.1 Structure and molecular weight characterization

NMR spectra were obtained using a Mercury 500 spectrometer. The polymers'

molecular weights were determined by gel permeation chromatography (GPC, HLC-8320GPC) and the calibration standard is polystyrene. All GPC measurements were carried out in $CHCl_3$ at 40 °C.

1.3.2 Thermal properties characterization

The thermal gravimetric analysis (TGA) and differential scanning calorimetry (DSC) were performed under nitrogen atmosphere (20 ml/min) using a Netzsch TGA (209F1) and Netzsch DSC (204F1) (heating rate: 10 ^oC/min). The DSC spectra were taken between 25 ^oC and 260 ^oC under N_2 protection for two cycles (heating rate: 10 ^oC/min).

1.3.3 Thin film structures characterization

Thin-film X-ray diffraction (XRD) experiments working at 3 KW were performed on a Powder X-ray Diffractometry (INCA Energy, Oxford Instruments). The films were prepared by drop-coasting of polymer solution (5 mg/ml in toluene).

1.3.4 UV/vis absorption spectra of monomer and polymers

UV/vis absorption spectra were recorded using a dual-beam grating Hitachi U-4100 absorption spectrometer. The solution UV/Vis absorption spectra of both monomers and polymers were recorded in chloroform at a standard concentration (0.1 mg/ml). The thin-film UV/Vis absorption spectra were measured for a spin-coated thin film (6 mg/ml polymers in chloroform on a quartz glass substrate, rotary speed: 1500 r/min).

1.3.5 Photoluminescence (PL) measurements

Photoluminescence (PL) measurements were conducted for two polymers in solution phase by the HITACHI fluorometer (F-4600) with an excitation wavelength at 600

nm. For the preparation of polymer solution samples, typically, 10 mg of the polymer was first dissolved in 25 mL chloroform. Then, 0.1 mL of the as-prepared polymer solution was added into the 4 mL mixture solvent of chloroform and methonal with different volume ratios, i.e., V_{CHCl3}: V_{MeOH} = 100:0; 87.5:12.5; 75:25; 62.5:37.5; 50:50; 37.5:62.5; 25:75; 12.5:87.5; 0:100).

2. Figures

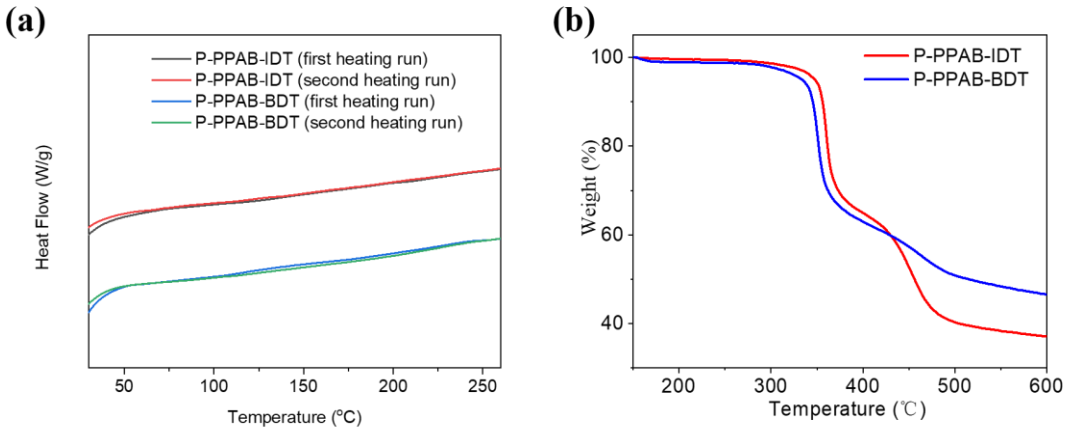

Figure S1. Two healing runs of DSC(a) and TGA curves(b) of polymers. (heating rate: 10 ℃ / min).

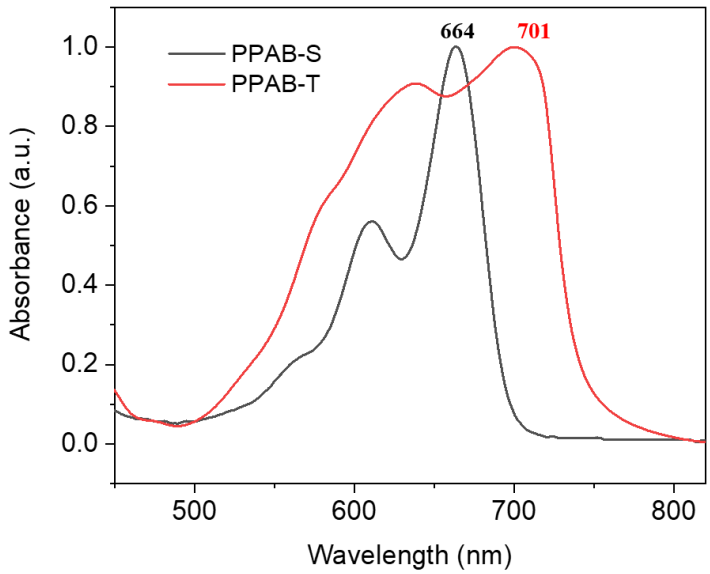

Figure S2. UV/vis absorption spectra of PPAB conjugated polymers in chloroform solution (S) and in thin film (T).

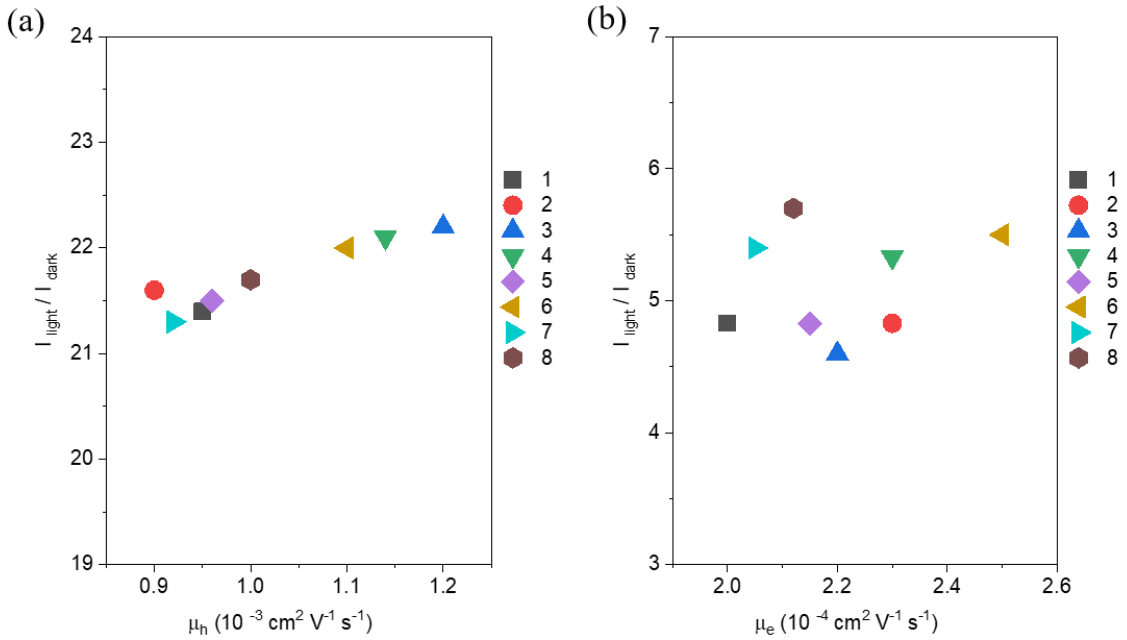

Figure S3. Summary of charge transport mobility and the I_{light}/I_{dark} ratios of the P-PPAB-BDT based on 8 different FETs (a, p-type; b: n-type)

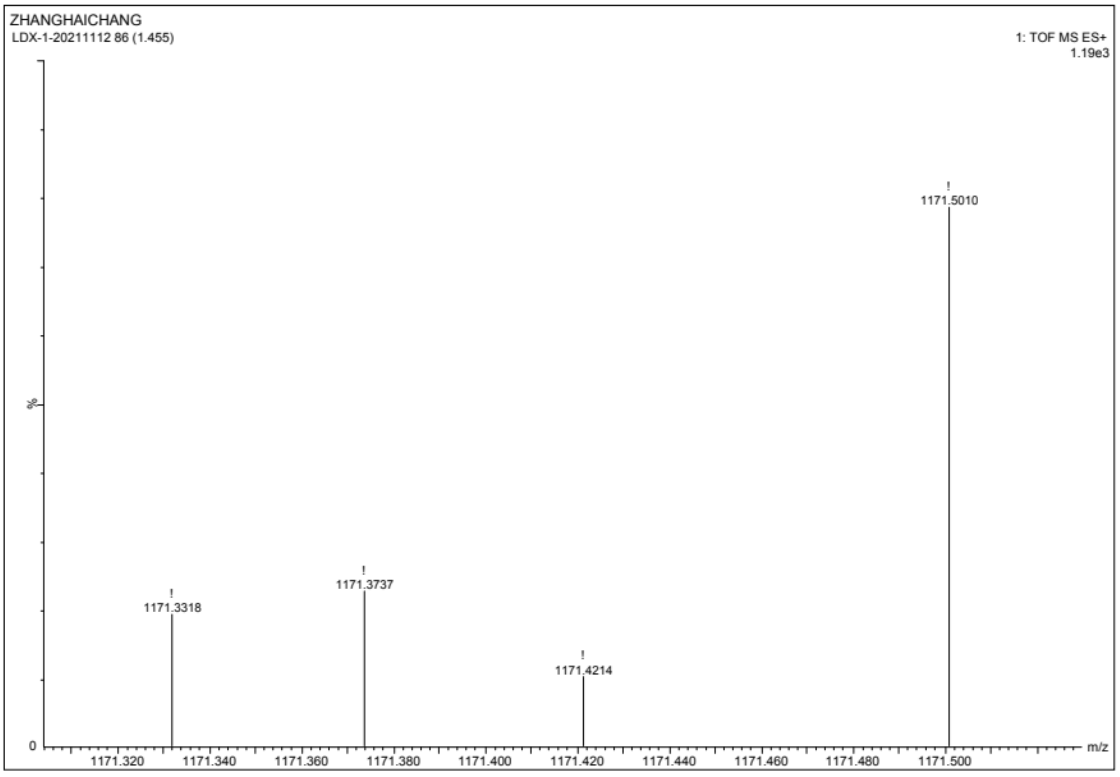

Figure S4. Mass spectrum (M+H+) of PPAB monomer.

3. Tables

Table S1. Optical and electrochemical properties of PPAB monomer, and P-PPAB-IDT and P-PPAB-BDT polymers.

Compounds	λ_{max} [nm]		HOMO	LUMO	E_g^{ec} / E_g^{opt}
	in solution	in thin film	[eV]	[eV]	[eV]
PPAB	664	701	5.47	3.94	1.53/1.65
P-PPAB-IDT	717	777	-5.30	-3.91	1.39/1.42
P-PPAB-BDT	691	723	5.37	-3.92	1.45/1.56

E_g^{ec} (electrochemical band gap) according to the following equation: $-E_{LUMO} = E_{onset(red)} + 4.8$ eV and $-E_{HOMO} = E_{onset(ox)} + 4.8$ eV, where $E_{onset(red)}$ and $E_{onset(ox)}$ are the onset potentials for the oxidation and reduction processes vs. ferrocene; E_g^{opt} (optical band gap) was measured at the onset of the absorption of organic molecules film ($E_g^{opt} = 1240/\lambda_{abs.onset}$ eV)

Table S2. Hole mobilities (μ_h), threshold voltage (V_{th}), and on/off ratios (I_{on}/I_{off}) of polymer-based FET device.

Polymers	Mobility ($cm^2 V^{-1} s^{-1}$)	V_{th} (V)	I_{on}/I_{off}	I_{off}
P-PPAB-IDT	2.3×10^{-2} (2.6×10^{-2})[a]	-23	10^3-10^4	1.9×10^{-8}
P-PPAB-BDT	1.1×10^{-3} (1.3×10^{-3})[a]	-31	10^4-10^5	3.9×10^{-10}
	2.2×10^{-4} (2.5×10^{-4})[b]	32	10^2-10^3	1.2×10^{-9}

The mobility was provided in the form of average (highest) and the performance is based on 8 different FETs. Mobility was extracted by fitting the linear part of the plot of $I_{DS}^{1/2}$ versus V_G using the equation $I_{DS} = C_i\mu(V_G - V_{Th})^2W/2L$. [a] hole mobility; [b] electron mobility.

4. Reference

1. Yuto Kage, Shigeki Mori, Marina Ide, *Mater. Chem. Front.* **2018**, 2, 112.